Small-Animal ^{18}F-FDG PET for Research on *Octopus vulgaris*: Applications and Future Directions in Invertebrate Neuroscience and Tissue Regeneration

Letizia Zullo[1], Ambra Buschiazzo[2], Michela Massollo[3], Mattia Riondato[4], Alessia Democrito[4], Cecilia Marini[2,4,5], Fabio Benfenati[1,6], and Gianmario Sambuceti[2,4,5]

[1]Center for Synaptic Neuroscience and Technology, Italian Institute of Technology, Genoa, Italy; [2]Division of Nuclear Medicine, Department of Health Science, University of Genoa, Genoa, Italy; [3]Nuclear Medicine Unit, EO Galliera Hospital, Genoa, Italy; [4]Nuclear Medicine Unit, IRCCS San Martino, Genoa, Italy; [5]Institute of Molecular Bioimaging and Physiology (IBFM), CNR, Milan, Italy; and [6]Department of Experimental Medicine, University of Genoa, Genoa, Italy

This study aimed to develop a method of administering ^{18}F-FDG to the common octopus in order to perform a PET biodistribution assay characterizing glucose metabolism in organs and regenerating tissues. **Methods:** Seven animals (two of which had a regenerating arm) were anesthetized with 3.7% $MgCl_2$ in artificial seawater and then injected with 18–30 MBq of isosmotic ^{18}F-FDG through either the left branchial heart or the anterior vena cava. After an uptake time of about 50 min, the animals were sacrificed and placed on the bed of a small-animal PET scanner, and 10-min static acquisitions were obtained at 3–4 bed positions to visualize the entire body. To confirm image interpretation, internal organs of interest were collected and counted with a γ-counter. **Results:** Administration through the anterior vena cava resulted in a good full-body distribution of ^{18}F-FDG as seen on the PET images. Uptake was high in the mantle mass and relatively lower in the arms. In particular, the brain, optic lobes, and arms were clearly identified and were measured for their uptake (SUV_{max}: 6.57 ± 1.86, 7.59 ± 1.66, and 1.12 ± 0.06, respectively). Interestingly, ^{18}F-FDG uptake was up to 3-fold higher in the highly proliferating areas of regenerating arms. **Conclusion:** This study represents a stepping-stone to the use of noninvasive functional techniques for addressing questions about invertebrate neuroscience and regenerative medicine.

Key Words: octopus; ^{18}F-FDG; micro-PET; functional imaging; regeneration

J Nucl Med 2018; 59:1302–1307
DOI: 10.2967/jnumed.117.205393

Cephalopods are among the most intelligent invertebrates, and they represent a class of highly specialized mollusks in which neural and morphologic novelties emerged together (*1,2*). Their behavioral capabilities and highly evolved neural system have prompted their recent inclusion in the list of species covered by European Union ethical regulations (*3–5*). For this reason, there is an increasing need for minimally invasive experimental approaches that, by reducing the impact of surgery, will allow functional investigation of the behavior, neurophysiology, and body function of live cephalopods. Octopuses are easily maintained and handled and are of an appropriate size for a canonical high-resolution small-animal PET system.

^{18}F-FDG PET is a widely used tool for the in vivo study of oncologic, cardiovascular, and neurologic disorders and of cerebral glucose metabolism (*6–9*). In view of the interest in developing novel strategies to repair bone and cardiovascular muscle, ^{18}F-FDG PET is also becoming relevant to studies of bone regeneration and cardiac repair and regeneration, because it allows following of tissue regeneration through noninvasive measurements of metabolic processes (*10–12*).

Animals use a variety of strategies for repair and regeneration of a lost function, leading to partial or full restoration. Given the limited regenerative capacity of mammals, these processes have historically been studied in nonmammalian vertebrates and invertebrates. The final aim is the discovery of common regeneration principles by which new therapeutic approaches in regenerative medicine can be developed.

Because of the great regenerative potential of the cephalopod mollusk *Octopus vulgaris,* it represents a viable alternative to vertebrate regeneration models. Cephalopods can regenerate lost or injured structures such as the shell, the appendages (arms and tentacles), the cornea, peripheral nerves, and brain centers (*13*). In particular, the arms of the octopus have a complex structure and physiology (*14–16*) that share similarities with early arm development and regeneration in some vertebrate models (*13,17,18*). These similarities make the octopus an ideal model for studying limb regeneration and for finding conserved pathways that might be triggered in various animal species (including mammals) to induce regeneration of injured tissue.

In this study, we developed a protocol for injecting a solution of ^{18}F-FDG into the venous system of *Octopus vulgaris* and then tested the use of a small-animal PET technique, common in the examination of higher vertebrates, to image glucose metabolism in the internal organs and regenerating limbs of the octopus. Blood circulation in coleoids is based on a completely closed and highly efficient system comprising a tripartite heart and a network of mostly contractile vessels that distribute the blood throughout the body (*19*). Relevant to our study, the presence of contractile blood vessels within the arms (*20*) ensures a good rate of blood

Received Nov. 20, 2017; revision accepted Feb. 12, 2018.
For correspondence or reprints contact: Letizia Zullo, Center for Synaptic Neuroscience and Technology, Istituto Italiano di Tecnologia, Largo Rosanna Benzi, 10, Torre D1, 16132, Genoa, Italy.
E-mail: letizia.zullo@iit.it
Published online Mar. 9, 2018.

flow even far from the heart and in the presence of high internal pressure, which often can occur in soft-bodied animals. We therefore evaluated the biodistribution of ^{18}F-FDG along the arms and the metabolic rate at the regenerating arm tips.

MATERIALS AND METHODS

The study and all procedures involving experimental animals were approved by the Institutional Review Board and by the Italian Ministry of Health (authorization 1111/2016-PR). Our research conformed with the ethical principles of the 3 Rs (replacement, reduction, and refinement) and of minimizing animal suffering, following directive 2010/63/EU (Italian legislative decree 26/2014) and the guidelines from Fiorito et al. (*5*).

Animal Treatment

Octopus vulgaris specimens of either sex were collected from the Ligurian coast during the spring and summer seasons of 2013 and 2017 and were placed in 80 × 50 × 45 cm marine aquaria. The tanks were filled with artificial seawater (ASW) and kept at a temperature of 18°C with a 12 h light/dark cycle. Water cleaning and oxygenation were ensured by a pump-filter and aeration system that continuously circulated the water through biologic filters. All relevant chemical and physical water parameters were constantly checked to prevent unhealthy or stress conditions. The animals were left to adapt to captivity for at least 10 d. Animals for the experiments were selected on the basis of a healthy shape (all arms and body parts intact), normal reflexes, voluntary movements such as arm extension and walking, regular eating, and motivation to attack prey (*4,5,21–23*).

The 2 experimental protocols used 7 animals (weight range, 150–450 g), two of which were also used in the regeneration study.

Regeneration Protocol

In 2 animals (animal 1, 150 g; animal 2, 182 g), the tip of the first left arm was surgically amputated to induce regeneration. Before the surgery, each animal was placed in 2% ethanol in ASW for about 5 min (*5,24,25*), until anesthetization was confirmed by a clear change in body patterns and posture, cessation of ventilation, unresponsiveness to external stimuli, and loss of righting reflex. Ethanol was the preferred anesthesia for this operation given that the duration of anesthesia would be brief and the recovery time is fast (*5*). No more than 10% of the total arm length was amputated, using fine scissors and cutting on a transverse plane. After surgery, the animals were placed back in their experimental tank, where they recovered from the anesthesia in about 2–5 min. The animals did not display behavioral modifications or signs of distress or suffering after the operation, and the amputated arm regenerated as in the natural environment (*4,5,25–27*). Regeneration was allowed for 11 d in animal 1 and 33 d in animal 2.

Biodistribution Analysis

The animals were anesthetized by the addition of $MgCl_2$ to ASW to a final concentration of 3.7%, received a single injection of radiotracer solution (200–300 μL of isosmotic ^{18}F-FDG, 18–30 MBq), and then were immediately transferred to a container without any $MgCl_2$ to prevent cessation of branchial ventilation and heartbeat and to facilitate radiotracer distribution through the body. The first experimental group comprised 3 animals whose injection was through the left branchial heart. The second experimental group comprised 4 animals whose injection was through the anterior vena cava; two of these were the animals that had undergone amputation. Both administration sites are upstream regarding the distribution of blood to organs (Fig. 1) (*5*). Following best-practice protocols, an uptake time of 50 min was used to maximize the chance that the radiotracer would reach the entire body. Indeed, in the standard protocol for humans and other studied models, uptake of ^{18}F-FDG in all organs is assumed to be complete by 50 min (*8,28*). The animals were then killed by being returned to the same ASW in which they had been injected, after the concentration of $MgCl_2$ had been increased to a fatal level. $MgCl_2$ was preferred because it produces simultaneous animal death and complete muscle relaxation, thus avoiding spontaneous reflex movements that can compromise the quality of scanning.

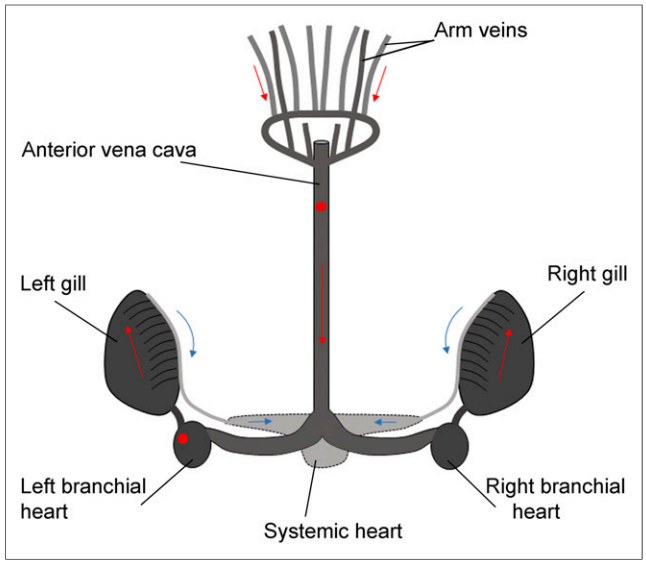

FIGURE 1. Left branchial heart and anterior vena cava locations (red circles) for injection into octopus venous system are upstream regarding distribution of blood to organs. Red arrows show blood returning from arms; blue arrows show oxygenated blood leaving gills.

The animals were then placed on the bed of a small-animal PET scanner (Albira; Bruker), and 10-min static acquisitions were obtained at 3 or 4 bed positions (depending on the total animal length). The animals were positioned so that the mantle, brain, and eyes were scanned in the first and second bed positions. PET data were reconstructed using maximum-likelihood expectation maximization. An experienced observer who was masked to experimental group identified a volume of interest in the studied organs to measure SUV_{max} (±SE). Internal organs of interest, hemolymph (cephalopod blood), brain, and muscle were sampled and weighted (solid organs were blotted dry), and their radioactivity was counted in a Cobra II γ-counter (Packard Bell) with the energy window set at 511 keV. Activity at nontarget sites was also measured to disclose possible contamination. The activity rate (in cpm) was determined with correction for the decay time between injection and counting. Counts were expressed as mean (±SE) percentage of the injected dose per gram of tissue (%ID/g). To assess the correlation between γ-counting and PET whole-body imaging, %ID/g was compared with SUV_{max}.

Statistical Analysis

Statistical analysis was performed using SigmaPlot, version 13.0 (Systat Software, Inc.). The distribution of the data was first assessed with a normality test (Shapiro–Wilk). Differences among datasets were verified by *t* testing and ANOVA. Kruskal–Wallis and Mann–Whitney rank sum were used as nonparametric tests. *P* values of less than 0.05 were considered significant.

RESULTS

Biodistribution Studies

γ-Counting. Octopus beak was chosen as a nontarget organ because it comprises mostly acellular chitin and therefore is not a

good site of radiotracer accumulation. Activity in the beak was accordingly low (0.19 ± 0.14 %ID/g; $n = 3$) (Fig. 2). Uptake in hemolymph ranged from about 0.4 to 3 %ID/g ($n = 3$), and uptake in excreted solution (sampled from the water bath in which the animal was held after injection and then brought to terminal anesthesia) was very low (0.013 ± 0.004 %ID/g; $n = 7$).

After left branchial heart injection (the first experimental group; $n = 3$), activity was high in the left branchial heart and gill (respectively, 11.72 ± 2.05 and 21.08 ± 3.40 %ID/g). Organs with a high metabolic rate, such as the brain and optic lobes, showed a good uptake level (respectively, 2.04 ± 0.28 and 5.37 ± 0.34 %ID/g). Several organs, such as the stomach, intestine, and hepatopancreas, displayed a high and variable level of accumulation (from ~1 to 12 %ID/g), probably because of their digestion-related functions. Uptake was low in muscle (0.54 ± 0.68 %ID/g). Organs directly receiving blood from the injected heart, such as the gills and optic lobes, showed the highest uptake (from ~5 to 21 %ID/g), with a marked increase on the side of the body that received the injection ($P < 0.05$, t test) (Fig. 2). Organs farther from the injection site did not show signs of lateralization ($P > 0.05$, ANOVA) (Fig. 2).

Because this lateralization might have prevented an even distribution of tracer to both body sides, in the second experimental group ($n = 4$) the injection was through the vena cava, which is located medially in the body and upstream from the branchial hearts. The vena cava is easy to access, and the intrinsic elasticity of the vein should help minimize radiotracer leakage from the injection point.

Small-Animal PET Scanning. As expected, a marked accumulation of radioactivity in the branchial heart was evident after left branchial heart injection (Figs. 3A and 3C) but not after vena cava injection (Figs. 3C and 3D). Organs with high metabolic activity, such as the central brain, optic lobes, and various internal organs, were clearly distinguishable for their high SUVs in both experimental groups (Figs. 3A and 3B). To quantify these data, we analyzed the SUVs of organs that were easily identifiable within the PET volume image with a very low scope for error.

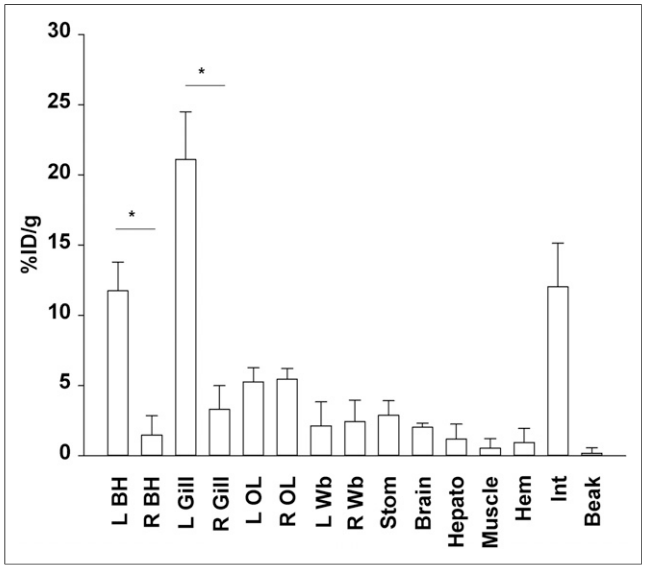

FIGURE 2. γ-counting analysis (mean and SE) of ^{18}F-FDG uptake in 3 animals receiving left branchial heart injection shows that uptake is highest in left branchial heart and gill (*$P < 0.05$, t test). Organs farther from injection site did not show lateralization ($P > 0.05$, ANOVA, Kruskal–Wallis). BH = branchial heart; OL = optic lobe; Wb = white body; Stom = stomach; Hepato = hepatopancreas; Hem = hemolymph; Int = intestine.

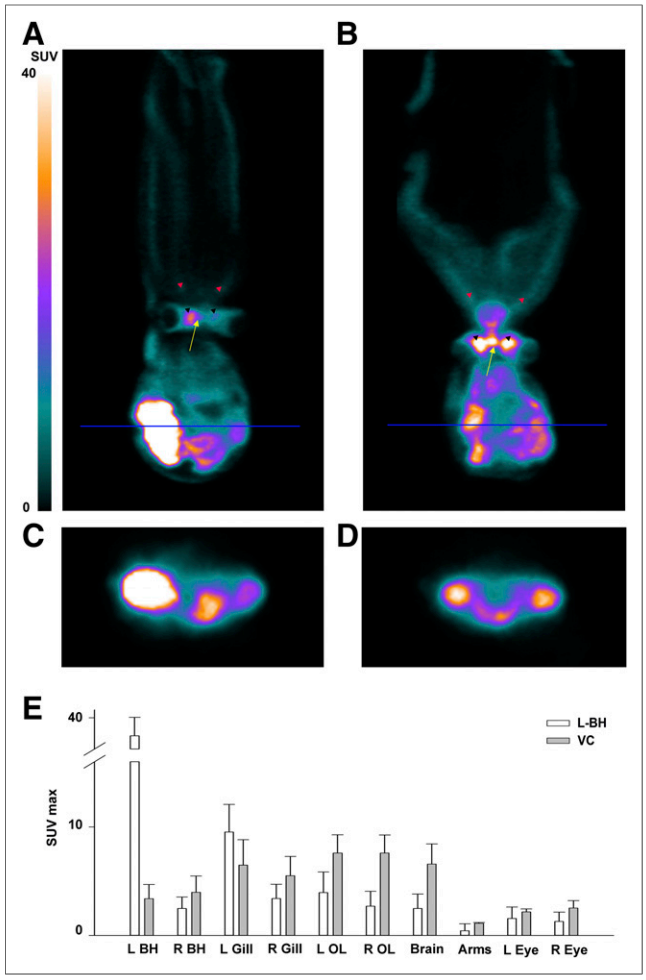

FIGURE 3. ^{18}F-FDG PET images showing that after both left branchial heart injection (A and C) and vena cava injection (B and D), high-metabolic-activity regions accumulate vast amounts of tracer. Accumulation in branchial heart (C and D) is more pronounced with left branchial heart injection than with vena cava injection. Arrows indicate central brain; black arrowheads, optic lobes; and red arrowheads, arms. (E) Plot of mean and SE for SUV_{max} in 3 animals receiving left branchial heart injection and 2 receiving vena cava injection. BH = branchial heart; OL = optic lobe; VC = vena cava.

We found that with left branchial heart injection, radioactivity was highest at the injected heart, immediately followed by the corresponding gill, but was markedly lower in the remaining organs (Fig. 3E). This pattern was especially evident when SUVs were compared between the vena cava group and the left branchial heart group, with the latter showing a generalized lower body uptake than the former (Fig. 3E). Hence, a considerable amount of radiotracer seems to remain in the injected heart, thus increasing the uptake measured both at the level of the branchial heart and at the level of the corresponding gill.

In detail, after left branchial heart administration, the brain and optic lobes showed a high SUV_{max} (2.49 ± 1.32 and 3.32 ± 1.83, respectively), whereas relative to nonneural areas, SUV_{max} was low at the level of the arms (0.44 ± 0.64) (Figs. 3A and 3E).

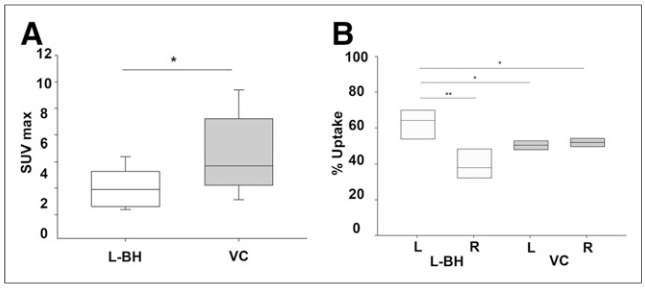

FIGURE 4. (A) SUV_{max} is lower after left branchial heart injection than after vena cava injection (*$P < 0.05$, Mann–Whitney rank sum test). (B) Percentage uptake on left side after left branchial heart injection is significantly higher than on right side (**$P < 0.01$, *t* test), as well as being higher than on either side after vena cava injection (*$P < 0.05$, *t* test). Median values are horizontal lines within bars. BH = branchial heart; VC = vena cava.

Animals receiving vena cava administration ($n = 2$) showed an SUV_{max} similarly high in the brain (6.57 ± 1.86) and optic lobes (7.59 ± 1.66) and low at the level of the arms (1.12 ± 0.06) (Figs. 3B and 3E). The low level of arm uptake can be explained by the fact that muscle energetics depend mostly on glycogen catabolism, whereas glycolysis accounts for only a small part of the muscle metabolic demand.

To estimate overall body uptake more clearly, we plotted the SUV_{max} distribution of the selected organs (excluding left branchial heart and gill, which might have been directly affected by residual injected radionuclide) in the 2 experimental groups. We found that vena cava injection produced significantly higher uptake than left branchial heart injection ($P < 0.05$, Mann–Whitney rank sum test; $n = 5$) (Fig. 4A).

We next calculated SUV separately for the left and right sides to address whether the injection method could cause lateralization of radiotracer diffusion and uptake. Interestingly, with vena cava administration, activity was evenly distributed between the two sides of the body, whereas with left branchial heart administration, activity was significantly higher on the left side ($P < 0.01$, *t* test; $n = 5$) (Fig. 4B), as well as being significantly higher than on either side after vena cava administration ($P < 0.05$, *t* test; $n = 5$) (Fig. 4B).

Overall, our data indicate that after vena cava injection the radioactive solution efficiently circulates throughout the body, reaches all organs, and is efficiently retained by organs with a higher metabolic rate.

^{18}F-FDG Uptake in Regenerating Arm

^{18}F-FDG PET scanning of the 2 animals with a regenerating arm showed that activity in the nonregenerating arms was higher at the central arm axes. This finding could be due to the massive population of neuronal cells that forms the peripheral nervous system of the arm and is located at its center. Like other neural structures, neurons of the peripheral nervous system consume a large amount of glucose to sustain their function and thus show high ^{18}F-FDG uptake. Activity in the regenerating arm was measured at 2 locations—the base and the tip—and was compared with activity in the nonregenerating arms of the same animal. Activity at the base of the stump was equal to that of the corresponding region in nonregenerating arms, whereas activity at the tip was 60% (animal 1) and 20% (animal 2) higher. We then measured the proximodistal extent of the high-metabolism areas and found it to reach to about 4 to 6 mm from the tip (Figs. 5A and 5B). At the stages of regeneration analyzed, the tip is populated by various quantities of intensely proliferating cells at the blastemal, nervous system, and muscle levels (Fig. 6) (*29*). In particular, cell proliferation at the tip is highest at around 11–17 d of regeneration and is lower at around 33 d, although still above basal levels (*29*). This factor might account for the large variability in increased uptake observed between the 2 regenerating arms. Vascular components are also present, but we believe them to have only an exiguous contribution to the measured activity, if any (Fig. 6). When vascular components were present, they reached a proximodistal area of up to only 1 mm (Fig. 6), whereas high uptake extended to 4–6 mm from the tip. In addition, the ^{18}F-FDG activity circulating in the hemolymph, which could potentially influence the radioactivity of a highly vascularized region or sinus, was measured right after scanning and was extremely low.

The high level of ^{18}F-FDG uptake observed in the regenerating arm tips might well reflect the presence of actively dividing cells in blastema, peripheral nervous tissue, and muscles, characteristic of regenerating tissues.

DISCUSSION

To the best of our knowledge, this has been the only study to use a labeled glucose analog to map metabolic activity in a cephalopod since the first such investigation, in 1992 (*30*). Several radiotracers were used in the late 1970s to assess protein synthesis in various invertebrates, including cephalopods. These investigations demonstrated the reliability of radiolabeling techniques to mark metabolically active organs such as gills, hearts, liver, hepatopancreas, brain, muscle, and even arm tips (*31–35*). The accumulation of radioactive compound was detected by liquid-scintillation counting and autoradiography, but both methodologies are limited by static detection and ex vivo use, and neither can answer questions about functional, in vivo, physiology.

^{18}F-FDG PET techniques allows high-resolution live scanning of highly metabolically active body regions and are widely used in clinical and preclinical studies in a variety of fields.

In particular, clinical imaging is an indispensable tool for characterizing damaged tissue in regenerative medicine. At present, only a few investigations are taking advantage

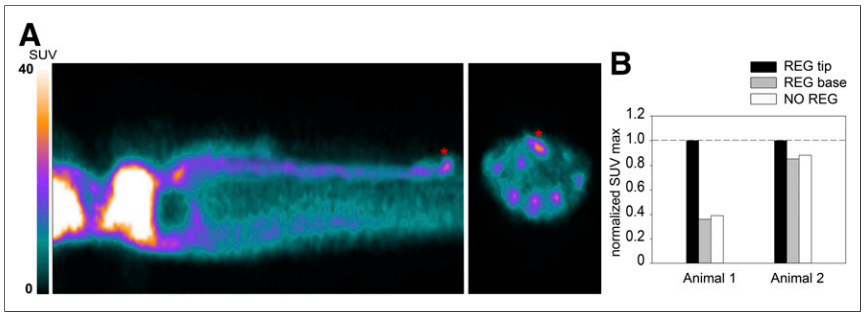

FIGURE 5. (A) ^{18}F-FDG PET image showing uptake (asterisks) at day 11 of regeneration in arm of animal 1. (B) SUV_{max} in normal nonregenerating arm and in regenerating arm tip and base after normalization to maximum arm uptake for each animal, on days 11 (animal 1) and 33 (animal 2) of regeneration. NO = normal; REG = regenerating.

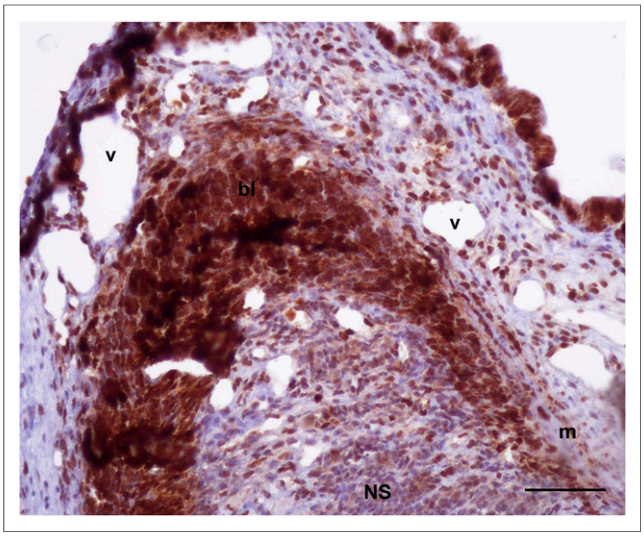

FIGURE 6. Histologic section of arm tip on day 17 of regeneration shows high proliferation rate (represented by brown precipitation after PCNA reaction), particularly in blastema (bl) region and in both nervous system (NS) and muscular system (m). Vascular components (v) are also present over proximodistal area up to 1 mm from arm tip (scale bar, 100 μm).

of this technique to assess and follow regenerative processes, especially regarding bone regeneration and cardiac remodeling (*10,11*).

Because of the innate constraints in using vertebrates to study regenerative ability, the application of alternative animal models has long been envisaged. Cephalopods such as octopods are renowned for their strong regenerative abilities and might serve as models for comparative regenerative investigations. In addition, cephalopods are endowed with a vertebratelike completely closed circulatory system working under high pressure, a characteristic that is unique among invertebrates and ensures fast and efficient blood flow throughout the body (*36,37*).

Because glucose metabolism in cephalopods is based on enzymes and reactions similar to those in higher animals, we assessed the use of the common ^{18}F-FDG PET clinical methodology to perform a full-body biodistribution assay on *Octopus vulgaris*.

Circulation in cephalopods is ensured by a vascular system and an aortic system; a pair of branchial hearts, each associated with a corresponding gill on each side of the body; and one central systemic heart (Fig. 1). In addition, a system of contractile veins ensures that the oxygenated blood reaches the central systemic heart, which in turn actively pumps it to the rest of the body. Blood pressure and flow rate in cephalopods circulate the total blood volume completely in approximately 120 s, thus distributing the tracer quickly (*38*). Here, we injected small doses of radionuclide directly into the venous system to achieve a full-body distribution. Uptake clearly lateralized through the branchial heart injection in organs immediately downstream from the injection location, as might be explained by the nature and structure of the octopus branchial heart, which is mainly nonmuscular and formed of a mass of spongy and poorly associated cells. Such a conformation might prevent rapid efflux of the tracer toward the circulatory system. After injection through the vena cava, there was no lateralization and uptake was higher throughout the body. This injection site is thus required to avoid radionuclide redistribution bias.

We based the injected dose on standard protocols for rats of similar weight, because of the similarity in blood volume (~5.8% of the animal wet weight, and an extracellular volume of 28%) and circulating glucose (on the order of 0.8–2 μmol/mL) between cephalopods and mammals (*39,40*). Glucose in cephalopods is an important fuel for all organs, including muscles, but is essential for the brain and heart, for which oxidation of blood glucose is the main energy source. Our imaging results well reflected the expected glucose distribution and consumption in the various organs. In particular, uptake was high in organs with a high metabolic rate, such as the brain, optic lobes, and heart, but low in the arms (which are mostly muscle).

We next wanted to test the sensitivity of ^{18}F-FDG PET in differentiating the metabolic activity of regenerating and nonregenerating arms. During early stages of arm morphogenesis, there is a massive presence of highly proliferating cells whose growth is largely dependent on fast, efficient energy production through glucose metabolism (*14,17,18,29,41*). Fully differentiated arm muscles in the adult at rest have a low growth rate and moderate hexokinase activity and rely more on glycogen catabolism (*35,42,43*). Therefore, regenerating tissue might accumulate labeled glucose at a higher rate than nonregenerating tissue.

Our detailed PET analysis showed that uptake was up to 3-fold higher in regenerating arms than in nonregenerating arms. Interestingly, a 3-dimensional reconstruction of the regenerating arms also showed that the location of the higher-metabolism areas matched that of highly proliferating muscular and undifferentiated tissue, as previously found in a fine-morphology investigation (*29*). The present findings might be an important step toward functional and molecular assessment of the regeneration process in various tissues and organs, as well as toward live visualization of nervous system activity. Achieving such an assessment would require repeated scanning of the animals to assess metabolic changes over time. Hence, it would be necessary to test recovery of the animal from the deep anesthesia under which it would be maintained for the entire scanning duration. Available data are encouraging, as they suggest that this species can be kept fully anesthetized for about 20 min (*5*). Moreover, the animal size can be downscaled to reduce the scanning time to 10–20 min (1 to 2 bed positions), and the animal can be covered with 3.7% $MgCl_2$ ASW–embedded tissue coats to prevent the skin and eyes from drying and help maintain prolonged anesthesia.

Further upgrades, such as the use of dynamic PET scanning and cell-specific radiolabeled compounds, can be envisaged to achieve various targets. This possibility would be particularly relevant in the field of behavioral neuroscience, by carrying the potential of linking in vivo brain activity to behavioral traits using minimally invasive investigations.

CONCLUSION

Standard small-animal ^{18}F-FDG PET imaging is a valuable tool for investigating metabolically active body regions at a single-organ resolution in the cephalopod mollusk *Octopus vulgaris*. Administration of the radioactive compound through the anterior vena cava is to be preferred for biodistribution studies in this animal, and this methodology can be used to assess regeneration in various regions of the body. Our study represents a first step toward the use of nuclear medicine imaging in emerging areas of research such as the neurobiology of invertebrates, with particular relevance in the field of regenerative medicine.

DISCLOSURE

No potential conflict of interest relevant to this article was reported.

ACKNOWLEDGMENTS

We thank Drs. Sara Maria Fossati and Arta Mehilli for technical help and animal maintenance.

REFERENCES

1. Albertin CB, Simakov O, Mitros T, et al. The octopus genome and the evolution of cephalopod neural and morphological novelties. *Nature.* 2015;524:220–224.
2. Lee PN, Callaerts P, de Couet HG, Martindale MQ. Cephalopod Hox genes and the origin of morphological novelties. *Nature.* 2003;424:1061–1065.
3. Berry A, Vitale A, Carere C, Alleva E. EU guidelines for the care and welfare of an "exceptional invertebrate class" in scientific research: Commentary. *Ann Ist Super Sanita.* 2015;51:267–269.
4. Fiorito G, Affuso A, Anderson DB, et al. Cephalopods in neuroscience: regulations, research and the 3Rs. *Invert Neurosci.* 2014;14:13–36.
5. Fiorito G, Affuso A, Basil J, et al. Guidelines for the Care and welfare of cephalopods in research: a consensus based on an initiative by CephRes, FELASA and the Boyd Group. *Lab Anim.* 2015;49:1–90.
6. Maya-Vetencourt JF, Ghezzi D, Antognazza MR, et al. A fully organic retinal prosthesis restores vision in a rat model of degenerative blindness. *Nat Mater.* 2017;16:681–689.
7. Phelps ME. Positron computed tomography studies of cerebral glucose metabolism in man: theory and application in nuclear medicine. *Semin Nucl Med.* 1981;11:32–49.
8. Sokoloff L, Reivich M, Kennedy C, et al. The [^{14}C]deoxyglucose method for the measurement of local cerebral glucose utilization: theory, procedure, and normal values in the conscious and anesthetized albino rat. *J Neurochem.* 1977;28:897–916.
9. Marini C, Salani B, Massollo M, et al. Direct inhibition of hexokinase activity by metformin at least partially impairs glucose metabolism and tumor growth in experimental breast cancer. *Cell Cycle.* 2013;12:3490–3499.
10. Naumova AV, Modo M, Moore A, et al. Clinical imaging in regenerative medicine. *Nat Biotechnol.* 2014;32:804–818.
11. Annibali S, Bellavia D, Ottolenghi L, et al. Micro-CT and PET analysis of bone regeneration induced by biodegradable scaffolds as carriers for dental pulp stem cells in a rat model of calvarial "critical size" defect: preliminary data. *J Biomed Mater Res B Appl Biomater.* 2014;102:815–825.
12. Sommese L, Zullo A, Schiano C, et al. Possible muscle repair in the human cardiovascular system. *Stem Cell Rev.* 2017;13:170–191.
13. Zullo L, Fossati SM, Imperadore P, Nodl MT. Molecular determinants of cephalopod muscles and their implication in muscle regeneration. *Front Cell Dev Biol.* 2017;5:53.
14. Fossati SM, Benfenati F, Zullo L. Morphological characterization of the Octopus vulgaris arm. *Vie Milieu.* 2011;61:197–201.
15. Zullo L, Fossati SM, Benfenati F. Transmission of sensory responses in the peripheral nervous system of the arm of Octopus vulgaris. *Vie Milieu.* 2011;61: 197–201.
16. Kier WM. The musculature of coleoid cephalopod arms and tentacles. *Front Cell Dev Biol.* 2016;4:10.
17. Fossati SM, Candiani S, Nodl MT, et al. Identification and expression of acetylcholinesterase in Octopus vulgaris arm development and regeneration: a conserved role for ACHE? *Mol Neurobiol.* 2015;52:45–56.
18. Nödl MT, Fossati SM, Domingues P, Sanchez FJ, Zullo L. The making of an octopus arm. *Evodevo.* 2015;6:19.
19. Wells MJ. Circulation in cephalopods. In: Saleuddind ASM, Wilbur KM, eds. *The Mollusca.* Vol. 5, Part 2. New York, NY: Academic Press; 1983:240–256.
20. Mislin H, Kauffmann M. The active vascular pulse in the arm-skin of cephalopods [in German]. *Rev Suisse Zool.* 1948;55:267–271.
21. Amodio P, Andrews P, Salemme M, Ponte G, Fiorito G. The use of artificial crabs for testing predatory behavior and health in the octopus. *ALTEX.* 2014;31:494–499.
22. Marini G, De Sio F, Ponte G, Fiorito G. Behavioral analysis of learning and memory in cephalopods. In: Byrne JH, ed. *Reference Module in Neuroscience and Biobehavioral Psychology.* Amsterdam, The Netherlands: Academic Press, Elsevier; 2017:441–462.
23. Maldonado H. The positive learning process in Octopus vulgaris. *Z Vgl Physiol.* 1963;47:191–214.
24. Andrews PLR, Tansey EM. The effects of some anesthetic agents in Octopus vulgaris. *Comp Biochem Physiol.* 1981;70C:241–247.
25. Crook RJ, Walters ET. Nociceptive behavior and physiology of molluscs: animal welfare implications. *ILAR J.* 2011;52:185–195.
26. Hague T, Florini M, Andrews PLR. Preliminary in vitro functional evidence for reflex responses to noxious stimuli in the arms of Octopus vulgaris. *J Exp Mar Biol Ecol.* 2013;447:100–105.
27. Andrews PLR, Darmaillacq AS, Dennison N, et al. The identification and management of pain, suffering and distress in cephalopods, including anaesthesia, analgesia and humane killing. *J Exp Mar Biol Ecol.* 2013;447:46–64.
28. Kiessling F, Pichler BJ, Hauff P. *Small Animal Imaging: Basics and Practical Guide.* New York, NY: Springer; 2017:237–245.
29. Fossati SM, Carella F, De Vico G, et al. Octopus arm regeneration: role of acetylcholine esterase during morphological modification. *J Exp Mar Biol Ecol.* 2013;447:93–99.
30. Novicki A, Messenger J, Budelmann B, et al. [^{14}C]deoxyglucose labelling of functional activity in the cephalopod central nervous system. *Proc Biol Sci.* 1992;249:77–82.
31. Thabrew MI, Poat PC, Munday KA. Carbohydrate metabolism in Carcinus maenas gill tissue. *Comp Biochem Physiol.* 1971;40B:531–541.
32. Storey KB, Storey JM. Octopine metabolism in the cuttlefish, Sepia officinalis: octopine production by muscle and its role as an aerobic substrate for nonmuscular tissues. *J Comp Physiol.* 1979;131:311–319.
33. Hochachka PW, Fields JHA. Arginine, glutamate, and proline as substrates for oxidation and for glycogenesis in cephalopod tissues. *Pac Sci.* 1982;36:325–335.
34. Garlick PJ, McNurlan MA, Preedy VR. A rapid and convenient technique for measuring the rate of protein synthesis in tissues by injection of ^{3}H phenylalanine. *Biochem J.* 1980;192:719–723.
35. Houlihan DE, McMillan DN, Agnisola C, et al. Protein synthesis and growth in Octopus vulgaris. *Mar Biol.* 1990;106:251–259.
36. Bertetti C. Contribution to knowledge of the vascular system in cephalopods [in Italian]. *Rend Accad Nazl XL.* 1956;6–7(ser 4):3–60.
37. Hill RB, Welsh JH. Heart, circulation, and blood cells. In: Wilbur KM, Yonge CM, eds. *Physiology of Mollusca.* Vol. 2. New York, NY: Academic Press; 1966:129.
38. O'Dor RK, Wells MJ. Circulation time, blood reserves and extracellular space in a cephalopod. *J Exp Biol.* 1984;113:461–464.
39. Storey KB, Storey JM, Johansen K, et al. Octopine metabolism in Sepia officinalis: effect of hypoxia and metabolite loads on the blood-levels of octopine and related-compounds. *Can J Zool.* 1979;57:2331–2336.
40. Goddard C, Martin A. Carbohydrate metabolism. In: Wilbur KM, Yonge CM, eds. *Physiology of Mollusca.* Vol. 2. New York, NY: Academic Press; 1966:275–308.
41. Fossati SM, Carella F, Benfenati F, et al. Octopus arm regeneration and its potential implication in reparative pathways. *J Shellfish Res.* 2011;30:1003.
42. Cory HT, Rose SPR. Glucose and amino acid metabolism in octopus optic and vertical lobes in vitro. *J Neurochem.* 1969;16:979–988.
43. Zammit VA, Newsholme EA. The maximum activities of hexokinase, phosphorylase, phosphofructokinase, glycerol phosphate dehydrogenases, lactate dehydrogenase, octopine dehydrogenase, phosphoenolpyruvate carboxykinase, nucleoside diphosphatekinase, glutamate-oxaloacetate transaminase and arginine kinase in relation to carbohydrate utilization in muscles from marine invertebrates. *Biochem J.* 1976;160:447–462.